Mol Neurobiol (2016) 53:5652–5663
DOI 10.1007/s12035-015-9480-z

Intranasal Delivery of RGD Motif-Containing Osteopontin Icosamer Confers Neuroprotection in the Postischemic Brain via $\alpha_v\beta_3$ Integrin Binding

Yin-Chuan Jin[1] · Hahnbie Lee[1,2] · Seung-Woo Kim[1,2] · Il-Doo Kim[1,2] · Hye-Kyung Lee[1,2] · Yunjin Lee[3] · Pyung-Lim Han[3] · Ja-Kyeong Lee[1,2]

Received: 19 June 2015 / Accepted: 8 October 2015 / Published online: 19 October 2015

Abstract Osteopontin (OPN) is a phosphorylated glycoprotein possessing an arginine-glycine-aspartate (RGD)-motif, which binds to several cell surface integrins and mediates a wide range of cellular processes. Inductions of OPN have been reported in the postischemic brain, and the neuroprotective effects of OPN have been demonstrated in animal models of stroke. In the present study, we showed a robust neuroprotective effect of RGD-containing icosamer OPN peptide (OPNpt20) in a rat model of focal cerebral ischemia (middle cerebral artery occlusion, MCAO). Intranasally administered OPNpt20 reduced mean infarct volume by 79.7 % compared to the treatment-naïve MCAO control animals and markedly ameliorated neurological deficits. In addition, OPNpt20 significantly suppressed the inductions of iNOS and of inflammatory markers in postischemic brains and in primary microglial cultures, demonstrating anti-inflammatory effects. Administration of a mutant peptide, in which RGD was replaced by arginine-alanine-alanine (RAA), failed to suppress infarct volumes in MCAO animals and co-administration of OPNpt20 with anti-$\alpha_v\beta_3$ integrin antibody failed to suppress iNOS induction in primary microglia culture, indicating that the RGD motif in OPNpt20 and endogenous $\alpha_v\beta_3$ integrin play critical roles. Furthermore, pull-down assay revealed a direct binding between OPNpt20 and $\alpha_v\beta_3$ integrin in primary microglia culture. Together, these results indicate that RGD-containing OPN icosamer has therapeutic potential in the postischemic brain and $\alpha_v\beta_3$ integrin-mediated anti-inflammatory effect might be an underlying mechanism.

Keywords Osteopontin · MCAO · Icosamer · Inflammation · RGD · Neuroprotection

Abbreviations

RGD	Arginine-glycine-aspartate
SLAY	Serine-leucine-alanine-tyrosine
RAA	Arginine-alanine-alanine
SLAA	Serine-leucine-alanine-alanine
OPN	Osteopontin
OPNpt20	20 amino acid peptide of osteopontin
OPNpt20-RAA	Mutant 20 amino acid peptide of osteopontin (in which RGD motif is replaced by RAA)
OPNpt20-SLAA	Mutant 20 amino acid peptide of osteopontin (in which SLAY motif is replaced by SLAA)
MCAO	Middle cerebral artery occlusion
mNSS	Modified neurological severity score
HUVECs	Human umbilical vein endothelial cells
GMS	Gelatin microsphere
SEM	Scanning electron microscope

Yin-Chuan Jin and Hahnbie Lee contributed equally to this work.

Electronic supplementary material The online version of this article (doi:10.1007/s12035-015-9480-z) contains supplementary material, which is available to authorized users.

✉ Ja-Kyeong Lee
jklee@inha.ac.kr

[1] Department of Anatomy, Inha University School of Medicine, 7-241 Shinheung-dong, Jung-Gu, Inchon 400-712, Republic of Korea

[2] Medical Research Center, Inha University School of Medicine, Inchon, South Korea

[3] Department of Brain and Cognitive Science, Ewha Womans University, Seoul, South Korea

Introduction

Osteopontin (OPN) is a phosphorylated glycoprotein that was initially considered to be an adhesive bone matrix protein but subsequently found to be a soluble cytokine [1]. OPN expression has been detected in various tissues, including bone, kidney, lung, liver, heart, brain, and most tumors, though it is worth noting that higher levels of expression have been reported in kidney and brain [2]. The induction of OPN has been reported in various physiological processes, for example, during gastrulation [3], and elevated OPN expression has also been observed in various pathological conditions, for example, in multiple sclerosis [4], rheumatoid arthritis [5], atherosclerosis [6], and asthma [7], in which its induction appears to be beneficial. In the central nervous system (CNS), OPN is expressed at low levels in neurons and microglia under normal conditions [8], but OPN expression is markedly upregulated in microglia and astrocytes under various pathological conditions, including Alzheimer's disease [9], Parkinson's disease [10], epilepsy [11], and stroke [8, 12].

OPN contains two main functional domains, an integrin-binding domain in its N-terminal and a CD44v-binding domain in its C-terminal, which are separated by a thrombin cleavage site [13]. An arginine-glycine-aspartic acid (RGD) motif in its integrin-binding domain binds to specific integrin receptors, such as, $\alpha_v\beta_3$, $\alpha_v\beta_5$, $\alpha_v\beta_1$, and $\alpha_8\beta_1$ [14]. In addition, SVVYGLR-containing domain, which is located right next to the RGD motif and exposed by thrombin cleavage, binds to $\alpha_9\beta_1$ and $\alpha_4\beta_1$ [15, 16]. OPN-integrin interactions mediate a wide range of cellular processes, which include cell adhesion, migration, and survival [14], and have been implicated in various disease processes. OPN also binds to CD44 hyaluronate receptor, a ubiquitous transmembrane glycoprotein that is known to mediate inflammatory processes, cell adhesion, and cell migration [17].

Regarding the therapeutic applications of OPN, the neuroprotective potency of exogenous administration of recombinant OPN protein has been examined, for example, in mouse brains exposed to transient focal ischemia [18, 19], in intracerebral hemorrhage mouse model [20, 21], in Parkinson's disease animal model [22], and in neonatal hypoxia-ischemia bran injury [23, 24]. We also reported neuroprotective effect of recombinant OPN protein in the postischemic brain and marked enhancement of the neuroprotective potency of OPN by delivering it via biodegradable gelatin microsphere [25]. Regarding the size and region of the effective OPN peptide, Doyle et al. (2008) [19] found that the 20 or even 10 amino acids OPN peptide harboring the RGD motif and SLAYGLR sequence had neuroprotective effect in a transient focal ischemia animal model.

This study was undertaken to examine the underlying molecular mechanisms of an OPN icosamer peptide containing the RGD motif and SLAYGLR sequence, which has been shown to confer a robust neuroprotective effect in middle cerebral artery occlusion (MCAO) animal model [19]. Importance of RGD motif and SLAYGLR sequence was determined by using two mutant peptides (RGD→RAA and SLAYGLR→SLAAGLR) in stroke animal model, and the interaction between OPN icosamer peptide and endogenous $\alpha_v\beta_3$ integrin was also examined in primary microglia culture. OPN icosamer peptide was delivered intranasally, and its neuroprotective effect, suppression of iNOS expression, and binding with endogenous $\alpha_v\beta_3$ integrin were compared with those of two mutant peptides.

Materials and Methods

Surgical Procedure Used for Middle Cerebral Artery Occlusion

Male Sprague–Dawley rats were housed under diurnal lighting conditions and allowed food and tap water ad libitum. All animal studies were carried out in strict accordance with the Guide for the Care and Use of Laboratory Animals published by the National Institute of Health and performed in accordance with ARRIVE guidelines (http://www.nc3rs.org/ARRIVE). The animal protocol used in this study was reviewed and approved by the INHA University-Institutional Animal Care and Use Committee (INHA-IACUC) with respect to ethicality (Approval Number INHA-110321-81). MCAO was carried out as previously described [26]. In brief, male Sprague–Dawley rats (250–300 g) were anesthetized with 5 % isoflurane in 30 % oxygen/70 % nitrous oxide and maintained using 0.5 % isoflurane in the same gas mixture during surgery. Occlusion of the right middle carotid artery was induced for 1 h by advancing a nylon suture (4–0; AILEE, Busan, South Korea) with a heat-induced bulb at its tip (~0.3 mm in diameter) along the internal carotid artery for 20–22 mm from the bifurcation of the external carotid artery. Reperfusion was allowed for up to 2 days. The left femoral artery was cannulated for blood sampling to analyze pH, PaO_2, $PaCO_2$, and blood glucose concentrations (I-STAT; Sensor Devises, Waukesha, WI). Regional cerebral blood flow (rCBF) was monitored using a laser Doppler flowmeter (Periflux System 5000; Perimed, Jarfalla, Sweden). Occlusion was considered successful if greater than 70 % reduction in cortical CBF occurred immediately after inserting an occluding suture. Animals were excluded if CBF was not reduced to less than 30 % of baseline during MCAO or blood flow was not restored during reperfusion. A thermoregulated heating pad and a heating lamp were used to maintain a rectal temperature of 37.0±0.5 °C during surgery. Animals were randomly allocated to seven groups; MCAO, treatment naïve MCAO control group (n=18), MCAO+OPNpt20, OPNpt20-administered MCAO group (n=35), MCAO+OPNpt20-

RAA, OPNpt20-RAA-administered MCAO group (n=7), MCAO+OPNpt20-SLAA, OPNpt20-SLAA-administered MCAO group (n=6), MCAO+rOPN, recombinant human OPN (rhOPN, R&D Systems, Minneapolis, MN)-administered MCAO group (n=4), Sham, sham-operated control group that have underwent surgery but not been subjected to MCAO (n=6), Sham+OPNpt20, OPNpt20-administered sham control (n=3). In general, mortality was not observed during surgery, but mortality after surgery was 6.3 % (5/80).

Infarct Volume Assessment

Rats were decapitated at 2 days post-MCAO, and whole brains were dissected coronally into 2-mm slices using a metallic brain matrix (RBM-40000, ASI, Springville, UT). Slices were immediately stained by immersion in 2 % 2,3,5-triphenyl tetrazolium chloride (TTC) at 37 °C for 15 min and then fixed in 4 % paraformaldehyde. Areas of infracted tissue in cortex and striatum were measured using the Scion Image program (Frederick, MD). To account for cerebral edema and differential shrinkage resulting from tissue processing, areas of ischemic lesions were determined by subtracting areas of ipsilateral hemispheres from those of contralateral hemispheres. Infarct volumes were calculated (in mm^3) by multiplying summed section infarct areas by section thickness.

Modified Neurological Severity Scores

Neurological deficits were evaluated using modified neurological severity scores (mNSS) at 2 days post-MCAO. The mNSS system consists of motor, sensory, balance, and reflex tests, all of which are graded using a scale of 0 to 18 [27], where higher scores represent more severe injury. Motor scores were determined by awarding scores to two items: (1) With a rat suspended by its tail, a score of zero or one was allocated for each sub-item (total score 0~3), that is, flexion of forelimbs, flexion of hindlimbs, head movement by>10° with respect to the vertical axis within 30 s; (2) A rat was placed on the floor, and scores from zero to three were allocated, that is, 0 for normal walking, 1 for an inability to walk straight, 2 for circling toward the paretic side, 3 for falling on the paretic side. Sensory tests included a placing test (score 0~1) and a proprioceptive test (score 0~1). For placing test, 0 for standing its ground with damaged forelimb on the edge of the table when gradually pushed toward there, 1 for fail to do that. For proprioceptive test, 0 for normal placing of forelimb on the edge of the table when forcefully contacting the dorsal surface of each forelimb with table edge, 1 for fail to do that. The beam balance test was used to test balance and scores from 0 to 6 were allocated as follows, balance with a steady posture, 0; grasping the side of the beam, 1; hugging the beam with one limb off the beam, 2; hugging the beam and two limbs off the beam or spinning around the beam over 60 s, 3; attempting to balance on the beam but falling off within 20 to 40 s, 4; attempting to balance on the beam but falling off within 20 s, 5; and making no attempt to balance or hang on to the beam, 6. Reflex testing scores were determined by awarding scores to the following four items (total score 0~4): pinna reflex, 0~1; corneal reflex, 0~1; startle reflex, 0~1; seizures, myoclonus, or myodystony, 0~1.

Rota-Rod Test

Twenty-four hours before MCAO, rats were conditioned on a rota-rod unit at a constant 3 rpm until they were able to remain on the rotating spindle for 180 s, and 24 h after MCAO, each rat was subjected to a test trial on the rota-rod at 5 rpm. Subsequently, residence times on the rota-rod at 10 and 15 rpm were measured hourly.

Intranasal Delivery

Intranasal administrations were carried out as previously described by Kim et al. (2012) [26]. In brief, rats were anesthetized with an intramuscular injection of a mixture of ketamine (3.75 mg/100 g body weight) and xylazine hydrochloride (0.5 mg/100 g body weight). The animals were randomly divided into six groups as mentioned in a previous section. A nose drop containing 100 ng of OPNpt20, OPNpt20-RAA, or OPNpt20-SLAA, or 2.86 μg of rhOPN in PBS (10 μl) was carefully placed in each nostril of anesthetized animals (supine 90° angle) using a pre-autoclaved pipet tip (T-200-Y, Axygen, CA). The procedure was repeated until the entire dosage had been administered with 2-min intervals between applications.

Immunohistochemistry

Animals were sacrificed at indicated times after MCAO, and brains were fixed in 4 % paraformaldehyde by transcardiac perfusion and post-fixed in the same solution overnight at 4 °C. Brain sections (20 μm) were obtained using a vibratome, and immunological staining was performed as previously described using a floating method [28]. Primary antibodies were diluted 1:500 for anti-ionized calcium binding adaptor molecule-1 (Iba-1) (Wako Pure Chemicals, Osaka, Japan) and 1:250 for anti-Mac-2 (Abcam, Cambridge, UK) antibodies. After washing with PBS containing 0.1 % Triton X-100, sections were incubated with anti-mouse IgG (Vector Laboratories, Burlingame, CA) for anti-Mac-2 or anti-rabbit IgG (Vector Laboratories, Burlingame, CA) for anti-Iba-1 in PBS for 1 h at room temperature and visualized using the HRP/3,3-diaminobenzidine (DAB) system. Experiments were repeated at least three times and representative images were presented.

Primary Microglia Culture

Primary microglial cultures were prepared as previously described [29]. In brief, cells dissociated from the cerebral hemispheres of 1-day-old postnatal rat brains (Sprague–Dawley strain) were seeded at a density of 1.2×10^6 cells/ml in Dulbecco's modified Eagle's medium (DMEM; Gibco, Carlsbad, CA) containing 10 % FBS (Hyclone, Logan, UT) and 1 % penicillin-streptomycin (Gibco, Carlsbad, CA). Two weeks later, microglia were detached from flasks by mild shaking and filtered through a cell strainer (BD Falcon, Bedford, MA) to remove astrocytes. After centrifugation (1000× *g*) for 5 min, cells were resuspended in fresh DMEM containing 10 % FBS and 1 % penicillin-streptomycin and plated at a final density of 1.5×10^5 cells/well on 24 multiwell culture plates. After 2 h, the medium was replaced with DMEM containing 5 % FBS and 1 % of B27 supplement (Gibco, Carlsbad, CA) and cultures were subjected to different treatments within 2 days.

NO Measurement

Primary microglia cells (1.5×10^5) were seeded in 24-well plates and 1 day later treated with LPS (100 ng/ml) for 24 h. To measure the amount of NO produced, 50 μl of conditioned medium was mixed with an equal volume of Griess reagent (0.5 % sulfanilamide, 0.05 % N-naphthalene-diamine-H-chloride, and 2.5 % H_3PO_4) and incubated for 5 min at room temperature. Absorbances of mixtures were measured at 550 nm using a microplate reader. $NaNO_2$ standards were used to calculate NO_2-concentrations.

siRNA Transfection

Rat osteopontin-specific small interfering RNA (siRNA) oligonucleotides (sc-270052, Santa Cruz Biotechnology, Santa Cruz, CA) were purchased from Dharmacon (Lafayette, CO). Transient transfections were carried out using Dharmafect 3 transfection reagent (Dharmacon, Lafayette, CO) according to manufacturer's protocol. siRNA and lipid complexes were added to wells to final concentration of 0.4 nM siRNA and 1 μl Dharmafect 3/well.

Real-Time PCR

RNA preparation and Real-Time PCR were performed as described previously. Total RNA was purified using TRI reagent (Sigma, St. Louis, MO), according to the manufacturer's instructions. First-strand complementary DNA (cDNA) was synthesized using the Takara RNA PCR kit (Takara Bio, Otsu, Japan) in a total volume of 20 μl containing 1 μg of total RNA. Real-time PCR was performed in a final volume of 20 μl containing 10 μl of 2× SYBR Green supermix (Takara Bio, Otsu, Japan), forward and reverse primers (1 μl each of 5 pmol/μl of both), and 5 μl of cDNA (50 ng; 1/100 dilution) using a Mini-Opticon Real-Time PCR System Detector (Bio-Rad, Richmond, CA). PCR was performed using 5 min at 95 °C, followed by 40 cycles of 30 s at 95 °C, 30 s at 57 °C, and 30 s at 72 °C. Specificity of amplification was determined by DNA melting curve analysis using built-in software. Differences in amplification fold were calculated by real-time PCR amplification of the target gene using GAPDH as an internal standard using the built-in Gene Expression Analysis software in the iCycler iQ Real-Time RCR Detection System (Bio-Rad, Richmond, CA). The following primer sets were used: 5′-CACCACGCTCTTCTGTCTACTG-3′ (forward) and 5′-GTACTTGGGCAGATTGACCTC-3′ (reverse) for TNF-α; 5′-GGAGAAGCTGTGGCAGCTA-3′ (forward) and 5′-GCTGATGTACCAGTTGGGGA-3′ (reverse) for IL-1β; 5′-GCTGTACAAGCAGTGGCAAA-3′ (forward) and 5′-GTCTGGAGTGGGAGGCACT-3′ (reverse) for COX-2; 5′-TCATTGACCTCAACTACATGGT-3′ (forward) and 5′-CTAAGCAGTTGGTGGTGCAG-3′ (reverse) for GAPDH; and 5′-GCATCCCAAGTACGAGTGGT-3′ (forward) and 5′-CCATGATGGTCACATTCTGC-3′ (reverse) for iNOS. Real-Time PCR was performed in quadruplicate.

Pull-Down Assay

Pull-down assay was performed using 20 μl (50 % slurry) of streptavidin agarose beads (Pierce, Rockford, IL). Biotinylated OPNpt20 (RGD) (0.1 or 1 nM; Peptron, Daejon, South Korea) or mutant OPNpt20 (RAA) (1 nM; Peptron, Daejon, South Korea) was incubated with recombinant $\alpha_v\beta_3$ integrin (Catalog # 3050-AV, R&D System, Minneapolis, MN) for 1 h in cell free condition or incubated with primary microglia cells for 3 h. Membrane proteins from primary microglia cultures were then extracted and incubated with streptavidin beads for 1 h at 4 °C with rotation, centrifuged at 8000 rpm for 1 min, washed three times, and analyzed by immunoblotting. Primary antibodies for anti-integrin alpha V (Abcam, Cambridge, UK) and anti-Na^+/K^+ ATPase (Abcam, Cambridge, UK) were detected using a chemiluminescence kit (Roche, Basel, Switzerland) using anti-rabbit HRP-conjugated secondary antibody (1:2000, Santa Cruz Biotechnology, Santa Cruz, CA).

Statistical Analysis

Two-sample comparisons were performed using the Student's *t* test and multiple comparisons using one-way or two-way analysis of variance (ANOVA). The analysis was performed using PRISM software 5.0 (GraphPad Software). Results are presented as means±SEM, and statistical difference was accepted at the 5 % level.

Results

Intranasally delivered RGD-containing OPN icosamer peptide (OPNpt20) suppressed infarct formation in the postischemic brain

The protective effects of OPNpt20 (IVPTVDVPNGRGDSLAYGLR) (Fig. 1a) were investigated in a rat model of focal cerebral ischemia induced by middle cerebral artery occlusion (MCAO). When OPNpt20 (10, 100, or 1000 ng) was administered intranasally at 1 h post-MCAO, mean infarct volumes at 2 days post-MCAO were reduced to 56.9±9.5 % (n=6, p<0.01), 29.2±6.0 % (n=6, p<0.01), and 26.2±4.6 % (n=6, p<0.01) versus that of treatment-naïve MCAO controls, respectively (Fig. 1b, c), indicating that OPNpt20 had a robust neuroprotective effect. When OPNpt20 (100 ng) was administered intranasally at 1, 3, or 6 h post-MCAO, mean infarct volumes at 2 days post-MCAO were reduced to 20.3±3.0 % (n=6, p<0.01), 51.3 ±7.3 % (n=6, p<0.01), and 87.1±6.4 % (n=5, p>0.05) versus that of treatment-naïve MCAO controls, respectively (Fig. 1d, e). Furthermore, no change in mean infarction volume was observed after administrating an equimolar amount of full length OPN (2.86 μg) at 3 h post-MCAO (Fig. 1d, e), indicating that OPNpt20 extended the therapeutic window. A mutant peptide containing the same 20 amino acids but with RGD replaced by RAA (OPNpt20-RAA, Fig. 1a) failed to reduce infarct volumes (91.2±12.7 %, n=6), when it (100 ng/rat) was administered intranasally at 1 h post-MCAO (Fig. 1f, g). However, another mutant peptide, in which SLAY was replaced by SLAA (OPNpt20-SLAA, Fig. 1a), reduced infarct volumes to levels similar to that of OPNpt20 (19.3±9.6 %, n=6, p<0.01) (Fig. 1f, g). These results indicate that OPNpt20 has robust neuroprotective effects in the postischemic brain and that the RGD motif is crucial for these neuroprotective effects. Physiological parameters, namely, pH, PaO_2, $PaCO_2$, and blood glucose, were similar in OPNpt20-treated animals and in treatment-naïve MCAO controls (Table 1).

OPNpt20 Improved Motor Impairment and Neurological Deficits After MCAO

In order to examine whether motor impairment is improved by OPNpt20, 100 ng OPNpt20 was administered at 1 h post-MCAO and modified neurological severity scores (mNSS) were determined at 2 days post-MCAO. mNSS were found to be markedly reduced in OPNpt20- (n=6, p<0.01) or

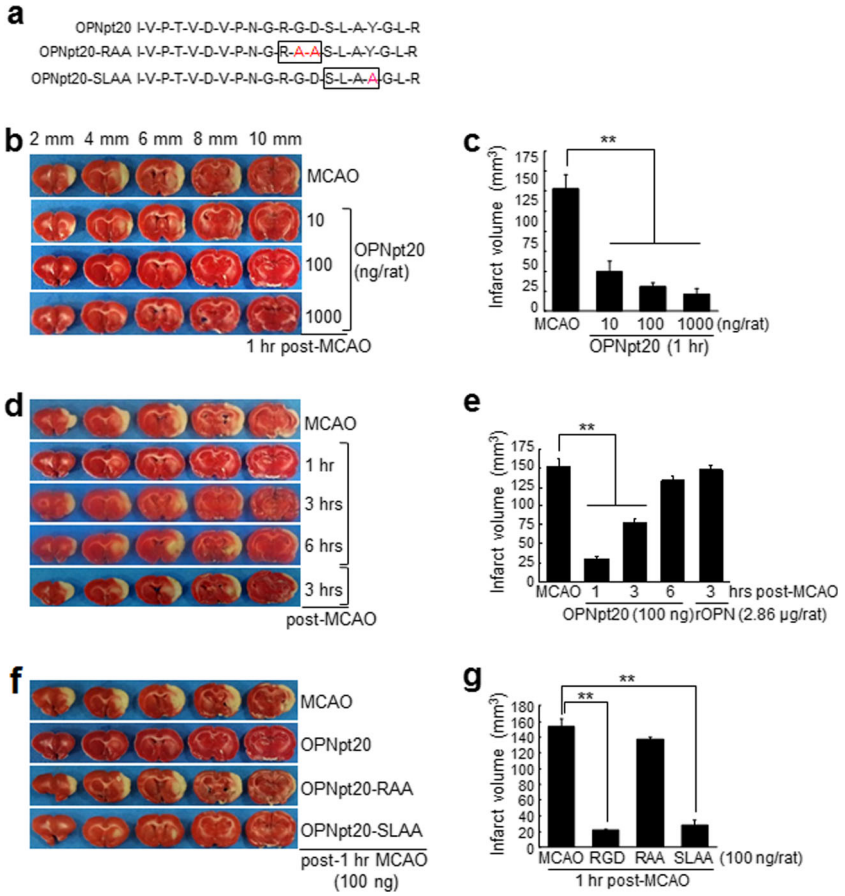

Fig. 1 Suppression of infarct volume by intranasal administration of OPNpt20 in the ischemic rat brain. **a** The sequences of OPNpt20 and of the two mutant peptides are shown. (**b**–**g**) OPNpt20 (10, 100, or 1000 ng) was administered intranasally at 1-h post-MCAO (**b**, **c**), and OPNpt20 (100 ng) was administered intranasally at 1, 3, or 6-h post-MCAO (**d**, **e**), and 100 ng of OPNpt20, OPNpt20-RAA, or OPNpt20-SLAA was administered intranasally at 1-h post-MCAO (**f**, **g**). TTC staining was carried out at 2 days post-MCAO. Representative images of infarctions are presented (**b**, **d**, **f**) and mean infarction volumes are presented as means±SEMs (n=4–6) (**c**, **e**, **g**). *MCAO* saline-treated MCAO rats, *OPNpt20* OPNpt20-treated MCAO rats, *RAA* OPNpt20-RAA-treated MCAO rats, *SLAA* OPNpt20-SLAA-treated MCAO rats, *rOPN* recombinant OPN-treated MCAO rats. **p<0.01

Table 1 Physiological parameters

	Treatment-naïve group		OPN pt20-treated group	
	Base	During ischemia	Base	During ischemia
Temperature, °C	37.3±0.3	37.2±0.1	37.2±0.2	37.1±0.4
pH	7.8±0.1	7.7±0.2	7.8±0.1	7.6±0.3
pO_2, mmHg	149.5±11.3	146.7±14.4	152.2±9.8	146.8±13.9
pCO_2, mmHg	36.4±1.9	37.3±1.4	39.1±0.5	38.6±2.3
Glucose, mg/dl	108.4±6.8	113.4±7.2	105.1±4.3	110.0±5.8

Values are means SD (n=3). One-way analysis of variance revealed no significant intergroup difference for any variance

OPNpt20-SLAA-treated animals but not in OPNpt20-RAA-treated animals compared to that in treatment-naïve MCAO controls (Fig. 2a). In addition, when motor activities were assessed at 2 days post-MCAO using the rota-rod test at 5 rpm, the mean time spent on the rota-rod by OPNpt20 (100 ng)-treated MCAO animals was significantly extended than in treatment-naïve MCAO controls (Fig. 2b). It was also extended by OPNpt20-SLAA-treated MCAO animals but not in OPNpt20-RAA-treated animals (Fig. 2b). Furthermore, the scores obtained from OPNpt20-treated MCAO animals at 10 and 15 rpm (with a 1 h interval between tests) were also significantly better than those of untreated MCAO controls (Fig. 2c, d). These results show that OPNpt20 improves motor impairment and neurological deficits and that the RGD motif is crucial for these effects.

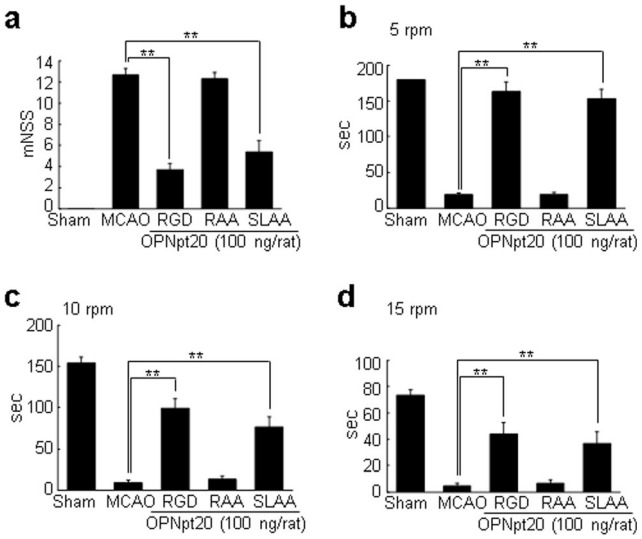

Fig. 2 Recovery of neurological and motor deficits by OPNpt20. OPNpt20 (100 ng), OPNpt20-RAA (100 ng), or OPNpt20-SLAA (100 ng) was administered intranasally at 1-h post-MCAO. **a** Neurological deficits were evaluated using modified neurological severity scores at 2 days post-MCAO. **b**–**d** The rota-rod test was performed at 5, 10, and 15 rpm at 2 days with a 1-h inter-trial interval. Data are presented as the means±SEMs (n=5–9). *Sham* sham-operated rats (n=5), *MCAO* treatment naive MCAO controls (n=6), *RGD* OPNpt20-treated MCAO rats (n=9), *RAA* OPNpt20-RAA-treated MCAO rats (n=7), *SLAA* OPNpt20-SLAA-treated MCAO rats (n=7)

Anti-Inflammatory Effects of OPNpt20 in the Postischemic Brain

To determine whether OPNpt20 confers anti-inflammatory effects in the postischemic brain, 100 ng of OPNpt20 was administered intranasally at 1 h post-MCAO and brain sections were stained with antibody against Iba-1, a marker of cells of myeloid origin, or Mac2, a marker of activated resident microglia at 2 days post-MCAO. In sham controls, Iba-1^+ cells were detected throughout brains, including contralateral hemispheres, and exhibited a ramified morphology (Fig. 3b). However, at 2 days post-MCAO, Iba-1^+ cells were rounded, indicating a phagocytic state in cortex (Fig. 3a, c). However, in OPNpt20 (100 ng, post-1 h)-administered MCAO animals, most Iba-1^+ cells retained a ramified morphology (Fig. 3d). In contrast to Iba-1^+ cells, Mac2^+ cells were barely detected in sham controls (Fig. 3e). At 2 days post-MCAO, numbers of Mac2^+ cells were markedly elevated in the cortical infarct cores of the treatment naïve-MCAO controls (Fig. 3f, h), but numbers of those were significantly smaller in the same regions of OPNpt20-treated animals (Fig. 3g, h). Furthermore, the administration of OPNpt20 at 1 h post-MCAO significantly suppressed the inductions of iNOS, TNFα, IL1-β, and COX-2 in ischemic hemispheres (black box in Fig. 3a) (Fig. 3i). Similar results were obtained in striata of OPNpt20-administered MCAO animals (Fig. S1). These results indicate that OPNpt20 suppresses inflammatory processes in the postischemic brain.

Exogenous OPNpt20 Suppressed NO Production in Activated Primary Microglia Cultures

To examine whether OPNpt20 suppresses NO production independent of neuroprotective effect, primary microglia

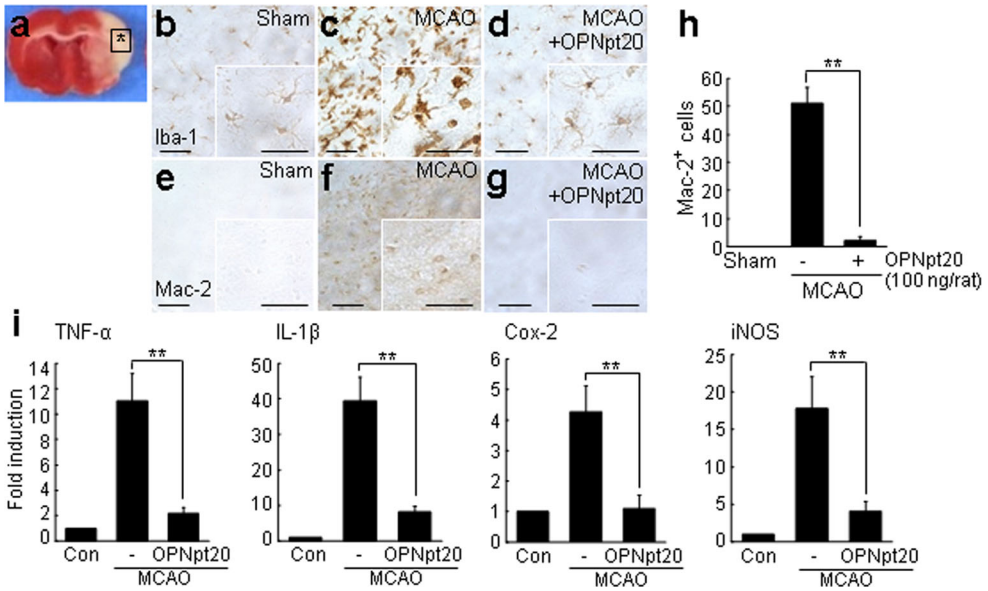

Fig. 3 Anti-inflammatory effects of OPNpt20 in the postischemic brain. OPNpt20 (100 ng) was administered intranasally at 1-h post-MCAO. **b**–**h** Coronal brain sections were prepared from cortices of ischemic hemispheres (**a**) at 2 days after sham operation (**b**, **e**) or MCAO (**c**, **d**, **f**, **g**) and processed for Iba-1 (**b**–**d**) and Mac-2 (**e**–**g**) immunostainings. Representative pictures from three independent experiments are presented (**b**–**g**) and numbers of $Mac2^{+}$-cells in regions (0.1 mm^2) around the *asterisk* in **a** were counted and presented as means±SEMs (n=12, 12 brain slices from 3 animals) (**h**). The insets in **b**–**g** are high magnification photographs of each image. *Scale bars* in **b**–**g** represent 400 μm, and those in *insets* represent 50 μm. **i** Samples for real-time PCR were prepared from the cortices of ischemic hemispheres as indicated in **a** (*box*) at 1 day post-MCAO. Levels of proinflammatory markers in the presence or absence of OPNpt20 are presented as means±SEMs (n=4). $^{**}p<0.01$

cultures were treated with LPS (100 ng/ml) in the presence of OPNpt20 and NO production was measured 24 h after LPS treatment. NO production was suppressed dose-dependently by OPNpt20 and at 10 nM, OPNpt20 reduced NO production by 48.9±4.1 % (n=4, $p<0.01$) of that in treatment-naïve LPS control cells (Fig. 4a). The same amount of OPNpt20-RAA failed to reduce NO production, but OPNpt20-SLAA (10 nM) reduced NO production by 39.0±4.2 % (n=4, $p<0.01$) (Fig. 4a). Similarly, iNOS induction was suppressed by OPNpt20 and by OPNpt20-SLAA but not by OPNpt20-RAA (Fig. 4b), indicating OPNpt20 suppresses iNOS expression in LPS-treated primary microglia cultures and that RGD plays a critical role. To confirm that exogenously delivered OPNpt20 is responsible for the iNOS suppression, endogenous OPN was knockdowned by OPN siRNA transfection (to 30.3±8.7 % of the normal level; Fig. 4c). We found that in siRNA-treated primary microglial cultures, iNOS expression was increased to 22.3-fold (n=3, $p<0.01$) of that in treatment-naïve control after LPS treatment, which was markedly greater than that in siRNA-untreated/LPS-treated control (8.7-fold, n=3, $p<0.01$) (Fig. 4d). However, no increment of iNOS induction was detected in non-target siRNA-transfected/LPS-treated primary microglial cultures compared to that in LPS only-treated cultures (Fig. 4d). Treatment of OPN siRNA-transfected/LPS-treated cultures with OPNpt20 (10 nM) markedly reduced iNOS expression (n=3, $p<0.01$) (Fig. 4d). Furthermore, similar suppression of iNOS induction in OPN siRNA-transfected/LPS-treated cultures was obtained after OPNpt20-SLAA (10 nM) treatment but not after OPNpt20-RAA (10 nM) treatment (Fig. 4d). Together, these results indicate that exogenously added OPNpt20 is capable of suppressing iNOS expression and that the RGD motif plays a critical role in this process.

Endogenous $\alpha_v\beta_3$ Integrin Plays a Critical Role in the OPNpt20-Mediated Suppression of iNOS Induction

Next, we examined the role of $\alpha_v\beta_3$ integrin in the OPNpt20-mediated suppression of NO production. Co-treatment of primary microglia cultures with anti-$\alpha_v\beta_3$ antibody (40 ng/ml) inhibited OPNpt20-mediated NO suppression, wherein nitrite production was suppressed only by 14.7±3.6 % (n=4, $p>0.05$) compared to that in LPS-treated cultures (Fig. 5a). Moreover, treatment of OPNpt20 (10 nM), after pre-incubating it with recombinant $\alpha_v\beta_3$ integrin (100 ng/ml) for 30 min, failed to suppress NO production (Fig. 5a). In contrast, OPNpt20 (10 nM)-mediated NO suppression in LPS-treated cells was detected after same amount of IgG treatment (Fig. 5a). Similarly, iNOS expression was not reduced after co-treating OPNpt20 with anti-$\alpha_v\beta_3$ antibody (40 ng/ml) or treating it after pre-incubating with recombinant $\alpha_v\beta_3$ integrin (100 ng/ml) for 30 min (Fig. 5b). These results indicate that $\alpha_v\beta_3$ integrin plays a critical role in OPNpt20-mediated iNOS suppression.

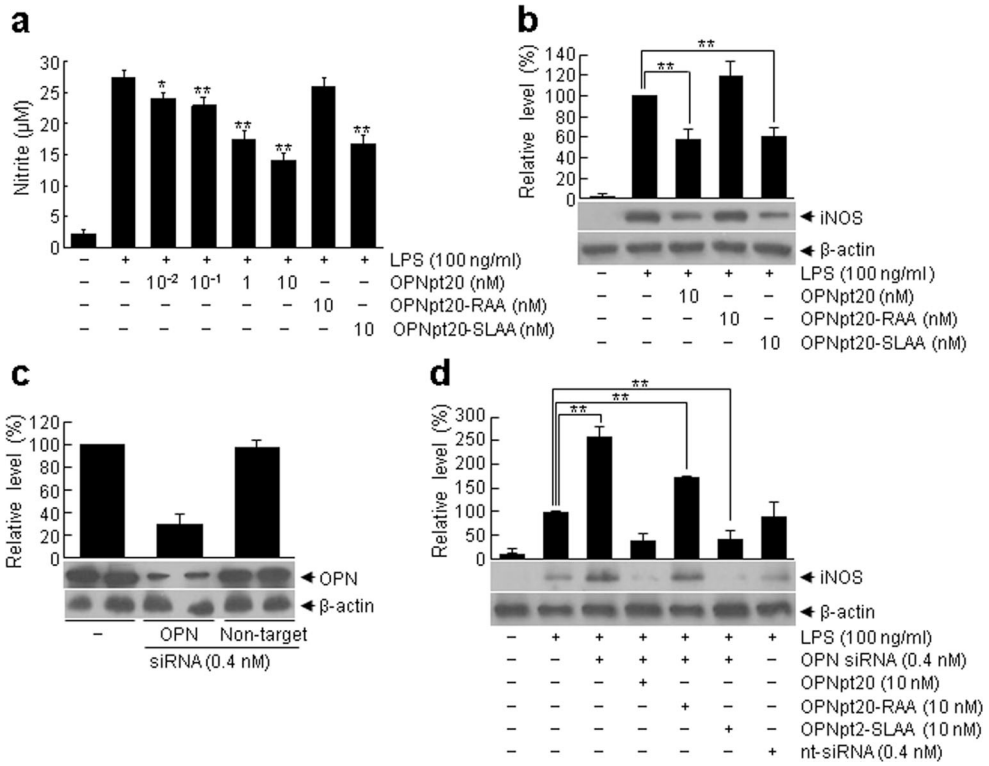

Fig. 4 Suppression of LPS-induced nitrite induction by exogenous OPNpt20 in primary microglial cultures. **a**, **b** Primary microglial cultures (1.5×10^5 cells/well) were pre-incubated with 0.01, 0.1, 1, or 10 nM of OPNpt20 or with 10 nM of OPNpt20-RAA or OPNpt20-SLAA for 1 h and then incubated with 100 ng/ml of LPS for 24 h. Nitrite production (**a**) and iNOS levels (**b**) were determined using a Griess assay and by immunoblotting, respectively, and results are presented as means±SEMs (n=3). **c** Primary microglia cultures were transfected with OPN siRNA (0.4 nM) or non-target siRNA (nt-siRNA, 0.4 nM) and levels of OPN in whole cell lysates were examined at 12 h after transfection by immunoblotting. **d** Twelve hours after OPN siRNA or nt-siRNA transfection, cells were treated with OPNpt20 (10 nM), OPNpt20-RAA (10 nM), or OPNpt20-SLAA (10 nM) for 1 h and then incubated with 100 ng/ml of LPS for 24 h. iNOS levels were then determined by immunoblotting. Results are presented as means±SEMs (n=3). **p<0.01 versus LPS-treated cells

OPNpt20 Interacted with Endogenous $\alpha_v\beta_3$ Integrin via its RGD Motif

To examine whether exogenously delivered OPNpt20 binds to endogenous $\alpha_v\beta_3$ integrin, pull-down assays were carried out using biotin-labeled OPNpt20. Cell free pull-down assay was carried out by incubating biotinylated-OPNpt20 and recombinant human $\alpha_v\beta_3$ integrin for 1 h at 4 °C, and samples were precipitated with biotin. Immunoblotting with anti-α_v integrin revealed that OPNpt20 bound to $\alpha_v\beta_3$ integrin and that this interaction was not observed when anti-$\alpha_v\beta_3$ antibody was co-incubated (Fig. 6a). To further confirm this interaction, membrane fractions were prepared from primary microglial cultures after 3 h of incubation with biotin-labeled OPNpt20 and pull-down assay was carried out. Results revealed that OPNpt20 (1 nM) bound to endogenous $\alpha_v\beta_3$ integrin and that this interaction showed dose-dependency (Fig. 6b). Markedly weak interaction of OPNpt20-RAA with endogenous $\alpha_v\beta_3$ integrin in both experiments demonstrated the specificity of the interaction (Fig. 6a, b). Uniform amounts of endogenous α_v and Na^+/K^+ ATPase in each lane served as input controls (Fig. 6a, b). Together, these results show that exogenously delivered OPNpt20 interacts with endogenous $\alpha_v\beta_3$ integrin and that the RGD domain of OPNpt20 is critical for this interaction.

OPNpt20 Suppressed the Inductions of Both Phosphorylated and Total STAT1 in LPS-Treated Primary Microglial Cultures in RGD Motif- and $\alpha_v\beta_3$ Integrin-Dependent Manners

We investigated whether OPNpt20 inhibits iNOS expression by promoting STAT1 degradation [30]. Nuclear phospho-STAT1 (pSTAT1) was markedly increased after treating primary microglia with LPS (100 nM, 24 h), but this induction significantly decreased in OPNpt20 (10 nM)/LPS-co-treated cells (Fig. 7a). This decrease was not detected when OPNpt20-RAA (10 nM) was used but was obtained when OPNpt20-SLAA (10 nM) was used (Fig. 7a). In addition, total STAT1 levels were also markedly increased in the whole cell lysates of LPS-treated cells and decreased in OPNpt20/LPS-co-treated cells, but this suppression was not observed in OPNpt20-RAA (10 nM)/LPS-co-treated cells (Fig. 7b). Similarly, OPNpt20-mediated suppressions of nuclear pSTAT1

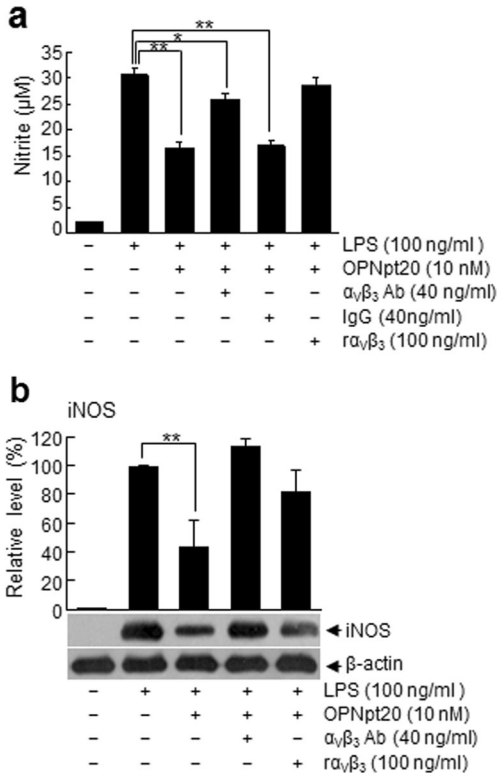

Fig. 5 $\alpha_v\beta_3$ integrin plays a critical role in OPNpt20-mediated suppression of LPS-induced nitrite induction in primary microglial cultures. Primary microglial cultures were incubated with OPNpt20 (10 nM) for 1 h in the presence of anti-$\alpha_v\beta_3$ antibody (40 ng/ml) ($\alpha_v\beta_3$ Ab) or incubated with OPNpt20 after pre-incubating it with recombinant $\alpha_v\beta_3$ ($r\alpha_v\beta_3$, 100 ng/ml) for 30 min and then incubated with 100 ng/ml of LPS for 24 h. Nitrite (**a**, n=4) and iNOS (**b**, n=4) levels were determined by using a Griess assay and by immunoblotting, respectively. Data are presented as means±SEMs. *p<0.05; **p<0.01 versus LPS-treated controls

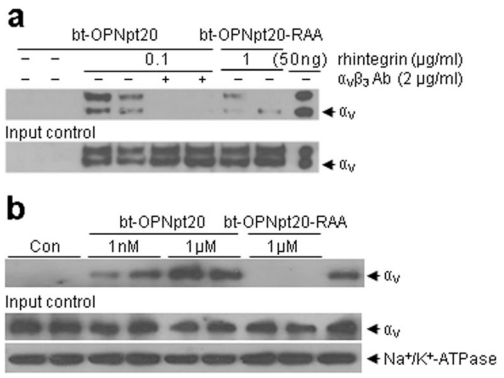

Fig. 6 Direct interaction between OPNpt20 and endogenous $\alpha_v\beta_3$ integrin in primary microglia cultures. **a** Biotinylated-OPNpt20 (bt-OPNpt20, 0.1 μg/ml) or biotinylated-OPNpt20-RAA (1 μg/ml) was incubated with recombinant human $\alpha_v\beta_3$ integrin (1 μg/ml) for 1 h. **b** Primary microglia cultures were incubated with biotinylated-OPNpt20 (bt-OPNpt20, 1 nM or 1 μM) or with biotinylated-OPNpt20-RAA (bt-OPNpt20-RAA, 1 μM) for 3 h, and membrane fractions were purified. **a**, **b** Pull-down assays were performed using streptavidin agarose beads, and immunoblotting was performed using anti-α_v antibody. Levels of endogenous α_v and Na+/K+ ATPase were used as input controls

induction and total STAT1 induction were prevented by co-treating anti-$\alpha_v\beta_3$ antibody (40 ng/ml) and by pre-incubating OPNpt20 with recombinant $\alpha_v\beta_3$ integrin protein (100 ng/ml) before treatment (Fig. 7c, d). These results indicate OPNpt20 suppressed the inductions of both phosphorylated and total STAT1 in LPS-treated cells and that the RGD motif in OPNpt20 and $\alpha_v\beta_3$ integrin play critical roles in this process.

Discussion

The present study demonstrates that the intranasal delivery of the RGD-containing OPN icosamer peptide, OPNpt20, exerts a robust neuroprotective effect in the postischemic brain, wherein RGD motif plays a critical role. We also showed that this icosamer peptide confers anti-inflammatory effect in primary microglia which was obtained by $\alpha_v\beta_3$ integrin-mediated suppression of iNOS induction. Although many authors have reported neuroprotective effects of OPN and showed the importance of RGD motif by using GRGDSP hexapeptide as a competitor [18, 21], this is the first report to demonstrate that the RGD motif is essential for these functions by using in vivo mutant analysis and to reveal molecular mechanism underlying these neuroprotective and anti-inflammatory effects by showing the interaction between exogenous OPN peptide and endogenous $\alpha_v\beta_3$ integrin in primary microglia culture.

Interestingly, in OPN-deficient mice, infarct volumes measured at 24 h after transient MCAO were found to be similar to those in wild-type mice [31], which contrast to the neuroprotective effects of recombinant OPN observed in the above-mentioned studies, in which OPN supplementation during the hyperacute period (immediately after or 10 min post-MCAO) suppressed infarct formation and mitigated neuronal damage [18, 19]. These contradictory observations can be explained by the delayed induction of OPN in various animal models of ischemia, for example, induction began at 24 h and peaked at 5 days in a mouse model of permanent focal ischemia [8, 12] and began at 24 h after reperfusion and peaked at 3 days in a transient forebrain ischemia rat model [32]. Therefore, since endogenous OPN is induced in a delayed manner, no significant changes were observed in infarct volume of the OPN-deficient mice measured at 24 h post-MCAO; however, exogenously delivered OPNpt20 during the acute period might "fill the gap" caused by the absence of endogenous OPN during this period, and thus, perform critical roles in the postischemic brain.

The present study also showed OPNpt20 had a greater therapeutic effect than full length OPN (Fig. 1b, c), which was probably due to the higher diffusability of the icosamer. In addition, considering the importance of the interaction between OPNpt20 and $\alpha_v\beta_3$ integrin, the increased potency of OPNpt20 might be due to the mobilization of its C-terminal,

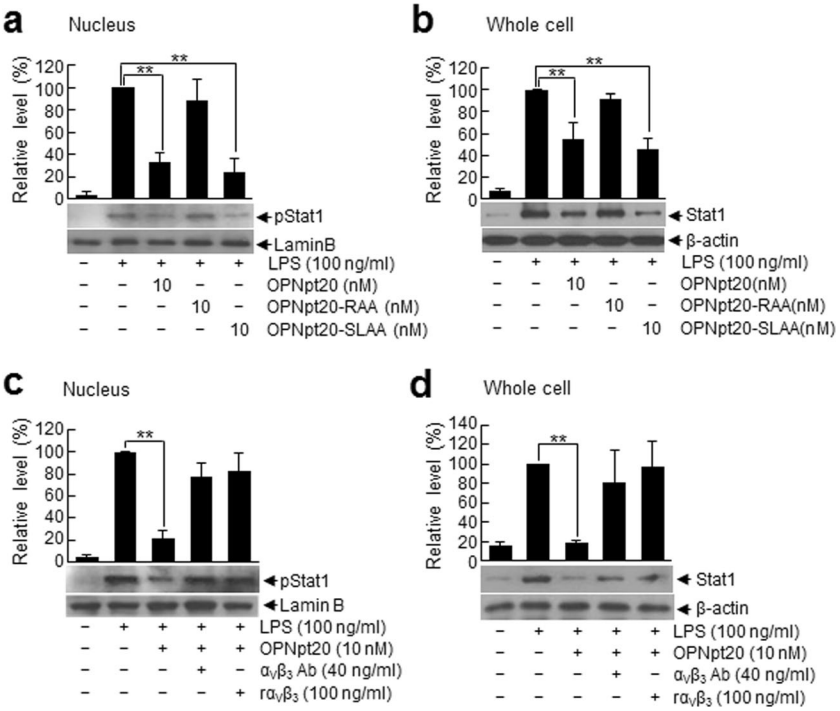

Fig. 7 Suppression of STAT1 expression and phosphorylation by OPNpt20 in LPS-treated primary microglial cells. **a**, **b** Primary microglia cultures were treated with OPNpt20 (10 nM), OPNpt20-RAA (10 nM), or OPNpt20-SLAA (10 nM) for 1 h and then treated with LPS (100 ng/ml). **c**, **d** Primary microglia cultures were co-treated with OPNpt20 (10 nM) and anti-$\alpha_v\beta_3$ antibody ($\alpha_v\beta_3$ Ab, 40 ng/ml) for 1 h or with OPNpt20 (10 nM) after pre-incubating it with recombinant $\alpha_v\beta_3$ ($r\alpha_v\beta_3$, 100 ng/ml) for 30 min (**c**, **d**) and then treated with LPS (100 ng/ml). Protein samples from nuclear extracts (**a**, **c**) or whole cell lysates (**b**, **d**) were prepared 24 h after LPS treatment, and immunoblot analyses were carried out using anti-phospho-STAT1 or anti-STAT1 antibodies, respectively. Representative immunoblots are presented, and levels of phospho-STAT1 and total STAT1 are presented as means± SEMs (n=3). $^{**}p<0.01$ versus LPS-treated cells

which facilitates the binding between the RGD motif and $\alpha_v\beta_3$ integrin. Although, the essential role played by the RGD motif in the reduction of iNOS expression has been reported in rat vascular tissue by Scott et al. (1998) [33], this is the first report to demonstrate that this process is mediated by integrin(s) by demonstrating direct binding between exogenous OPNpt20 and endogenous $\alpha_v\beta_3$ integrin and by mutant analysis. It is interesting to note that the same interaction was detected in HUVECs (data not shown), indicating that this binding is not limited by tissue type but rather a general phenomenon. The downstream signaling pathways connecting OPN/integrin and modulation of STAT1 phosphorylation and iNOS level need further study. Regarding post-translational modifications, although phosphorylation state of OPN has been reported to be important for its function [19, 34], no phosphorylation sites were localized within the peptide we used in the present study. In addition, possible signaling pathways for OPNpt20 via interacting with integrin members other than $\alpha_v\beta_3$, for examples, $\alpha_v\beta_1$, $\alpha_v\beta_5$, or $\alpha_8\beta_1$, also need further study.

Regarding the importance of the SLAYGLR motif, it has been reported that this motif increases the scope of integrin binding by OPN to $\alpha_4\beta_1$ and $\alpha_9\beta_1$ [15, 16] and that it plays an important role in various disease processes. However, in the present study, we found that the SLAYGLR motif plays no role in infarct suppression or in iNOS suppression because replacement of SLAY in the SLAYGLR motif with SLAA had no effect on OPNpt20-mediated infarct volume reduction (Fig. 1d, e), on OPNpt20-mediated suppression of iNOS induction (Fig. 4b, d), or on OPNpt20-mediated STAT1 and pSTAT1 suppressions (Fig. 7a, b). This lack of dependency on the SLAYGLR motif was surprising. It is interesting to note here that recently, Kale et al., (2014) [35] reported enhanced angiogenesis and tumor growth through $\alpha_9\beta_1$ integrin, which has been shown to bind SLAYGLR motif [15] but not via αvβ3 integrin in a RGD-independent manner. Therefore, we believe that functional importance of specific motifs might depend on the different cell types and animal models used or to specificities of effects involved and this issue required further study.

In addition to its anti-inflammatory effects, OPN is known to act as an attractant and inducer that drives the lateral migration of neuroblasts from the subventricular zone to the ischemic region [36]. In addition, OPN is known to exert anti-apoptotic effects [37] and to scavenge toxic substances, for examples, excess Ca^{2+} and dead neurons [38, 39] in the postischemic brain. Although studies are required to determine whether OPNpt20 also performs the above-mentioned

functions, we found that OPNpt20 has pro-angiogenic effect (In preparation, Jin and Lee). In view of the fact that stroke leads to brain injury via a complex series of pathophysiological events, treatment with a therapeutic peptide like OPNpt20, that targets multiple mechanisms, offers advantages. Furthermore, OPNpt20 is derived from an endogenous protein and, therefore, is probably free of safety concerns.

Acknowledgments This work was financially supported by a Medical Research Center Grant 2014R1A5A2009392 (to J.-K.L.) funded by the National Research Foundation (NRF) of Korea.

References

1. Denhardt DT, Giachelli CM, Rittling SR (2001) Role of osteopontin in cellular signaling and toxicant injury. Annu Rev Pharmacol Toxicol 41:723–749
2. Platzer G, Schedlbauer A, Chemelli A, Ozdowy P, Coudevylle N, Auer R et al (2011) The metastasis-associated extracellular matrix protein osteopontin forms transient structure in ligand interaction sites. Biochemistry 50:6113–6124
3. Thayer JM, Giachelli CM, Mirkes PE, Schwartz SM (1995) Expression of osteopontin in the head process late in gastrulation in the rat. J Exp Zool 272:240–244
4. Steinman L, Martin R, Bernard C, Conlon P, Oksenberg JR (2002) Multiple sclerosis: deeper understanding of its pathogenesis reveals new targets for therapy. Annu Rev Neurosci 25:491–505
5. Xu G, Nie H, Li N, Zheng W, Zhang D, Feng G et al (2005) Role of osteopontin in amplification and perpetuation of rheumatoid synovitis. J Clin Invest 115:1060–1067
6. Ohsuzu F (2004) The roles of cytokines, inflammation and immunity in vascular diseases. J Atheroscler Thromb 11:313–321
7. Xanthou G, Alissafi T, Semitekolou M, Simoes DC, Economidou E, Gaga M et al (2007) Osteopontin has a crucial role in allergic airway disease through regulation of dendritic cell subsets. Nat Med 13:570–578
8. Wang X, Louden C, Yue TL, Ellison JA, Barone FC, Solleveld HA et al (1998) Delayed expression of osteopontin after focal stroke in the rat. J Neurosci 18:2075–2083
9. Wung JK, Perry G, Kowalski A, Harris PL, Bishop GM, Trivedi MA et al (2007) Increased expression of the remodeling- and tumorigenic-associated factor osteopontin in pyramidal neurons of the Alzheimer's disease brain. Curr Alzheimer Res 4:67–72
10. Iczkiewicz J, Rose S, Jenner P (2007) Osteopontin expression in activated glial cells following mechanical- or toxin-induced nigral dopaminergic cell loss. Exp Neurol 207:95–106
11. Borges K, Gearing M, Rittling S, Sorensen ES, Kotloski R, Denhardt DT et al (2008) Characterization of osteopontin expression and function after status epilepticus. Epilepsia 49:1675–1685
12. Ellison JA, Velier JJ, Spera P, Jonak ZL, Wang X, Barone FC et al (1998) Osteopontin and its integrin receptor alpha(v)beta3 are upregulated during formation of the glial scar after focal stroke. Stroke 29:1698–1707
13. He B, Mirza M, Weber GF (2006) An osteopontin splice variant induces anchorage independence in human breast cancer cells. Oncogene 25:2192–2202
14. Standal T, Borset M, Sundan A (2004) Role of osteopontin in adhesion, migration, cell survival and bone remodeling. Exp Oncol 26:179–184
15. Yokosaki Y, Matsuura N, Sasaki T, Murakami I, Schneider H, Higashiyama S et al (1999) The integrin alpha(9)beta(1) binds to a novel recognition sequence (SVVYGLR) in the thrombin-cleaved amino-terminal fragment of osteopontin. J Biol Chem 274:36328–36334
16. Bayless KJ, Meininger GA, Scholtz JM, Davis GE (1998) Osteopontin is a ligand for the alpha4beta1 integrin. J Cell Sci 111:1165–1174
17. Weber GF, Ashkar S, Glimcher MJ, Cantor H (1996) Receptor-ligand interaction between CD44 and osteopontin (Eta-1). Science 271:509–512
18. Meller R, Stevens SL, Minami M, Cameron JA, King S, Rosenzweig H et al (2005) Neuroprotection by osteopontin in stroke. J Cereb Blood Flow Metab 25:217–225
19. Doyle KP, Yang T, Lessov NS, Ciesielski TM, Stevens SL, Simon RP et al (2008) Nasal administration of osteopontin peptide mimetics confers neuroprotection in stroke. J Cereb Blood Flow Metab 28:1235–1248
20. Wu B, Ma Q, Suzuki H, Chen C, Liu W, Tang J et al (2011) Recombinant osteopontin attenuates brain injury after intracerebral hemorrhage in mice. Neurocrit Care 14:109–117
21. Suzuki H, Hasegawa Y, Chen W, Kanamaru KT, Zhang JH (2010) Recombinant osteopontin in cerebral vasospasm after subarachnoid hemorrhage. Ann Neurol 68:650–660
22. Iczkiewicz J, Broom L, Cooper JD, Wong AM, Rose S, Jenner P (2010) The RGD-containing peptide fragment of osteopontin protects tyrosine hydroxylase positive cells against toxic insult in primary ventral mesencephalic cultures and in the rat substantia nigra. J Neurochem 114(6):1792–1804
23. Chen W, Ma Q, Suzuki H, Hartman R, Tang J, Zhang JH (2011) Osteopontin reduced hypoxia-ischemia neonatal brain injury by suppression of apoptosis in a rat pup model. Stroke 42(3):764–769
24. van Velthoven CT, Heijnen CJ, van Bel F, Kavelaars A (2011) Osteopontin enhances endogenous repair after neonatal hypoxic-ischemic brain injury. Stroke 42(8):2294–2301
25. Jin Y, Kim IY, Kim ID, Lee HK, Park JY, Han PL et al (2014) Biodegradable gelatin microspheres enhance the neuroprotective potency of osteopontin via quick and sustained release in the post-ischemic brain. Acta Biomater 10(7):3126–3135
26. Kim ID, Shin JH, Kim SW, Choi S, Ahn J, Han PL et al (2012) Intranasal delivery of HMGB1 siRNA confers target gene knockdown and robust neuroprotection in the postischemic brain. Mol Ther 20:829–839
27. Chen J, Sanberg PR, Li Y, Wang L, Lu M, Willing AE et al (2001) Intravenous administration of human umbilical cord blood reduces behavioral deficits after stroke in rats. Stroke 32:2682–2688
28. Kim JB, Lim CM, Yu YM, Lee JK (2008) Induction and subcellular localization of high-mobility group box-1 (HMGB1) in the postischemic rat brain. J Neurosci Res 86:1125–1131
29. Kim JB, Sig Choi J, Yu YM, Nam K, Piao CS, Kim SW et al (2006) HMGB1, a novel cytokine-like mediator linking acute neuronal death and delayed neuroinflammation in the postischemic brain. J Neurosci 26:6413–6421
30. Gao C, Guo H, Mi Z, Grusby MJ, Kuo PC (2007) Osteopontin induces ubiquitin-dependent degradation of STAT1 in RAW264.7 murine macrophages. J Immunol 178:1870–1881
31. Schroeter M, Zickler P, Denhardt DT, Hartung HP, Jander S (2006) Increased thalamic neurodegeneration following ischaemic cortical stroke in osteopontin-deficient mice. Brain 129:1426–1437
32. Choi JS, Kim HY, Cha JH, Choi JY, Lee MY (2007) Transient microglial and prolonged astroglial upregulation of osteopontin following transient forebrain ischemia in rats. Brain Res 1151:195–202
33. Scott JA, Weir ML, Wilson SM, Xuan JW, Chambers AF, McCormack DG (1998) Osteopontin inhibits inducible nitric oxide

synthase activity in rat vascular tissue. Am J Physiol 275:H2258–H2265
34. Li H, Shen H, Yan G, Zhang Y, Liu M, Fang P et al (2015) Site-specific structural characterization of O-glycosylation and identification of phosphorylation sites of recombinant osteopontin. Biochim Biophys Acta 1854(6):581–591
35. Kale S, Raja R, Thorat D, Soundararajan G, Patil TV, Kundu GC (2014) Osteopontin signaling upregulates cyclooxygenase-2 expression in tumor-associated macrophages leading to enhanced angiogenesis and melanoma growth via α9β1 integrin. Oncogene 33(18):2295–2306
36. Yan YP, Lang BT, Vemuganti R, Dempsey RJ (2009) Osteopontin is a mediator of the lateral migration of neuroblasts from the subventricular zone after focal cerebral ischemia. Neurochem Int 55:826–832
37. Ophascharoensuk V, Giachelli CM, Gordon K, Hughes J, Pichler R, Brown P et al (1999) Obstructive uropathy in the mouse: role of osteopontin in interstitial fibrosis and apoptosis. Kidney Int 56: 571–580
38. Shin YJ, Kim HL, Choi JS, Choi JY, Cha JH, Lee MY (2011) Osteopontin: correlation with phagocytosis by brain macrophages in a rat model of stroke. Glia 59:413–423
39. Shin YJ, Kim HL, Park JM, Cho JM, Kim CY, Choi KJ et al (2012) Overlapping distribution of osteopontin and calcium in the ischemic core of rat brain after transient focal ischemia. J Neurotrauma 29: 1530–1538